

Trajectory-based non-adiabatic simulations of the polariton relaxation dynamics

Cite as: J. Chem. Phys. 162, 124113 (2025); doi: [10.1063/5.0246099](https://doi.org/10.1063/5.0246099)

Submitted: 30 October 2024 • Accepted: 10 March 2025 •

Published Online: 27 March 2025



View Online



Export Citation



CrossMark

Deping Hu,^{1,a)} Benjamin X. K. Chng,² Wenxiang Ying,³ and Pengfei Huo^{3,4,5,b)}

AFFILIATIONS

¹ Center for Advanced Materials Research, Beijing Normal University, Zhuhai 519087, China

² Department of Physics and Astronomy, University of Rochester, Rochester, New York 14627, USA

³ Department of Chemistry, University of Rochester, 120 Trustee Road, Rochester, New York 14627, USA

⁴ The Institute of Optics, Hajim School of Engineering, University of Rochester, Rochester, New York 14627, USA

⁵ Center for Coherence and Quantum Optics, University of Rochester, Rochester, New York 14627, USA

Note: This paper is part of the JCP Special Topic on Algorithms and Software for Open Quantum System Dynamics.

^{a)} Electronic mail: depinghu@bnu.edu.cn

^{b)} Author to whom correspondence should be addressed: pengfei.huo@rochester.edu

ABSTRACT

We benchmark the accuracy of various trajectory-based non-adiabatic methods in simulating the polariton relaxation dynamics under the collective coupling regime. The Holstein–Tavis–Cummings Hamiltonian is used to describe the hybrid light–matter system of N molecules coupled to a single cavity mode. We apply various recently developed trajectory-based methods to simulate the population relaxation dynamics by initially exciting the upper polariton state and benchmark the results against populations computed from exact quantum dynamical propagation using the hierarchical equations of motion approach. In these benchmarks, we have systematically varied the number of molecules N , light–matter detunings, and the light–matter coupling strengths. Our results demonstrate that the symmetrical quasi-classical method with γ correction and spin-mapping linearized semi-classical approaches yield more accurate polariton population dynamics than traditional mixed quantum-classical methods, such as the Ehrenfest and surface hopping techniques.

Published under an exclusive license by AIP Publishing. <https://doi.org/10.1063/5.0246099>

I. INTRODUCTION

Molecular cavity quantum electrodynamics (QED) systems, which contain strongly interacting molecules with quantized cavity photonic modes, are emerging quantum systems that exhibit new phenomena in chemistry and physics.^{1–8} Previous theoretical studies have shown that these hybrid light–matter states, so-called polaritons,^{2–4,9–11} can modify chemical reactions via light–matter coupling.^{3,4,10,12–14} In addition, recent experiments have shown that molecular polaritons have drastically different transport properties compared to their bare excitonic components, paving the way for efficient and scalable optoelectronic devices based on polaritons.^{15–20} The light–matter hybridization also partially reduces the influence of phonons on the polariton because the photon component does not couple to the phonon. This leads to the polaron decoupling effect^{21,22} and the well-known absorption line shape narrowing.^{23,24}

In particular, coupling N molecular exciton states with a quantized cavity mode produces two polariton states, commonly referred to as the upper polariton (UP) and lower polariton (LP) states, each containing light and matter excitation characters. There are $N - 1$ remaining excitonic dark states (DS) that do not mix with photonic states or have a significant transition dipole from the ground state and are thus optically dark. Upon photoexcitation to the UP, the system will quickly relax to the DS and slowly transition to the LP.^{25,26} Polariton relaxation dynamics play a crucial role in understanding the polariton photoluminescence spectra,^{26–29} understanding the relative lifetime of the polariton and dark states,^{25,27} interpret the sub-average behavior of motional narrowing,³⁰ and the transition rates between the polariton and dark states,²⁵ as well as the corresponding decoherence process.³¹

To study polariton relaxation dynamics, one often uses the Holstein–Tavis–Cummings (HTC) Hamiltonian^{6–8,21,26,32} to model

the interplay between the exciton, photon, and phonon degrees of freedom (DOF). The HTC model couples many molecules, which are described as two-level systems, to both a cavity photon mode and phonon modes that are added phenomenologically to the molecules. In the strong-coupling regime, it has been shown that the HTC Hamiltonian captures the underlying physics of the cavity-QED systems,^{7,26,33–37} such as the polariton's relaxation dynamics^{7,25,26,36} and the polaron decoupling effect between excitons and their corresponding phonon modes.^{23,38}

A popular approach to simulate the non-adiabatic dynamics of systems with coupled electronic–nuclear degree of freedom is the mixed quantum-classical (MQC) methods,^{39–42} which has been widely used to model polariton relaxation dynamics.^{6–8} Two commonly used MQC methods are the mean-field Ehrenfest method (MFE)⁴³ and the surface hopping method.^{44,45} These methods treat the electronic DOF quantum mechanically while propagating the nuclear DOF classically (while often sampling the initial condition through quantum Wigner distributions). To simulate the dynamics of molecular polaritons, one extends the MQC approaches to treat both the electronic and photonic DOF quantum mechanically while propagating the nuclear DOF classically.^{5–8,46–52} However, the mixed quantum-classical approximations built into these methods have been known to produce unphysical results, such as the breakdown of detailed balance (that is, the long-term populations) for the MFE method⁵³ and the introduction of artificial electronic coherence or incorrect chemical kinetics for the surface hopping method.⁵⁴

To address the shortcomings of the MQC approaches above, other non-adiabatic dynamics methods have been developed in the diabatic representation, several of which are based on mapping formalism.^{55,56} For example, methods such as the linearized semi-classical initial value representation (LSC-IVR),^{57,58} partially linearized density matrix (PLDM) method,^{59,60} symmetrical quasi-classical (SQC) method,^{61,62} and the quantum-classical Liouville equation (QCLE) method^{63,64} are developed based on the Meyer–Miller–Stock–Thoss (MMST) mapping formalism.^{55,65,66} Furthermore, methods such as the spin-mapped linearized semi-classical (spin-LSC)^{67–69} and the spin-mapped partially linearized density matrix (spin-PLDM) method^{70,71} are derived from the recently developed generalized spin-mapping formalism, which uses the generalized spin-mapping relations to describe the electronic DOF⁶⁸ while using a linearized approximation for the nuclear DOF.^{72,73} These methods have shown significant improvements in numerical results over existing MQC approaches, such as in characterizing the population dynamics of spin-boson models,⁶⁷ exciton dynamics in light-harvesting complexes,⁶⁸ *ab initio* on-the-fly simulations,^{74–78} exciton–polariton quantum dynamics,⁵¹ and vibrational polariton quantum dynamics.⁴² Generalized quantum master equation (GQME)⁷⁹ is also shown to significantly improve the accuracy of the semi-classical population dynamics, taking advantage of the short-lived, more accurate memory kernels computed from these trajectory-based methods. Recently, these non-adiabatic semiclassical mapping dynamics methods are also benchmarked against the tensor-train thermo-field dynamics approach.^{80,81} From these previous results, these non-adiabatic dynamical methods based on mapping formalism should also outperform MQC methods in simulating the polariton relaxation dynamics, although there have been limited investigations into the efficacy of these methods for polaritonic systems.^{23,26,27,42,82,83}

Despite much recent progress on using MQC methods to model exciton polariton relaxation dynamics^{6–8} in *ab initio* atomistic systems, there is no existing work on accessing the accuracy of these trajectory-based methods on polariton relaxation dynamics under the collective coupling regime, with simple model systems where the numerically exact results are available. There is, however, a recent work on using trajectory-based method on simulating vibrational polariton dynamics under the single molecule limit.⁴² In this paper, we use the Ehrenfest method, global flux surface-hopping (GFSH) method,⁸⁴ SQC method with corrected zero-point energy (γ -SQC),⁸⁵ and spin-LSC method^{88,69} to simulate the population dynamics of a system that is initially excited into the UP state. These methods are benchmarked with the numerically exact hierarchical equations of motion (HEOM) approach.^{86–88} Numerical results are presented for HTC models with different physical parameters, such as the number of molecules that are coupled to the cavity mode, the single-molecule coupling strength, the light–matter detunings, and various parameters for the phonon bath. Our results provide valuable information on the accuracy of the commonly used MQC methods and the recently developed mapping approaches for simulating polariton relaxation dynamics in the HTC model.

II. THEORY AND METHODS

A. The Holstein–Tavis–Cummings QED Hamiltonian

We use the Holstein–Tavis–Cummings (HTC) Hamiltonian^{1,22,26,89,90} to model the polariton dynamics in the collective coupling regime. The total Hamiltonian can be separated into a component describing the system term \hat{H}_S , a component describing the bath term \hat{h}_B , and a system–bath interaction term \hat{H}_{SB} . This separation of terms is expressed as

$$\hat{H}_{\text{HTC}} = \hat{H}_S + \hat{h}_B + \hat{H}_{SB}. \quad (1)$$

In the remainder of this paper, we use units $\hbar = 1$ for convenience.

The system term \hat{H}_S consists of the excitonic DOF of the molecules and the photonic DOF of the cavity and is further expressed as^{31,91}

$$\hat{H}_S = \hat{H}_M + \hat{H}_{\text{cav}} + \hat{H}_{LM}, \quad (2)$$

where \hat{H}_M describes the matter contribution due to the excitonic DOF, \hat{H}_{cav} describes the cavity contribution, and \hat{H}_{LM} is the light–matter interaction term. The matter contribution \hat{H}_M to the Hamiltonian describes N identical and non-interacting molecules. We label these molecules as $n \in (0, N - 1)$. Each molecule is modeled as an effective two-level system that represents the molecule's ground and excited states, written as

$$\hat{H}_M = (\omega_0 + \lambda) \sum_{n=0}^{N-1} \hat{\sigma}_n^\dagger \hat{\sigma}_n, \quad (3)$$

where $\hat{\sigma}_n^\dagger = |e_n\rangle\langle g_n|$ and $\hat{\sigma}_n = |g_n\rangle\langle e_n|$ creates and annihilates an excitation on the n th molecule, respectively, with $|g_n\rangle$ and $|e_n\rangle$ as the ground and excited states for molecule n , and ω_0 is the excitation energy between the molecule's ground and excited state. The corresponding reorganization energy λ is due to exciton–phonon

coupling, which is described in the system–bath interaction \hat{H}_{SB} [see Eq. (7)].

The quantized radiation mode of the cavity is expressed as

$$\hat{H}_{\text{cav}} = \omega_c \left(\hat{a}^\dagger \hat{a} + \frac{1}{2} \right), \quad (4)$$

where ω_c is the photon frequency of the cavity mode, and \hat{a}^\dagger and \hat{a} are the creation and annihilation operators for a photon in the cavity mode, respectively. Here, we consider only a single cavity mode interacting with the molecules.

For the light–matter interaction term \hat{H}_{LM} , we assume the long-wavelength approximation, that is, each molecule is coupled to the quantized radiation field with the same light-matter coupling strength g_c . Assuming the rotating wave approximation, \hat{H}_{LM} is expressed as

$$\hat{H}_{\text{LM}} = g_c \sum_{n=0}^{N-1} \left(\hat{a}^\dagger \hat{\sigma}_n + \hat{a} \hat{\sigma}_n^\dagger \right). \quad (5)$$

The bath Hamiltonian \hat{h}_{B} in Eq. (1) describes the nuclear DOF, which we assume is a phonon environment that consists of a set of identical, non-interacting harmonic oscillators,

$$\hat{h}_{\text{B}} = \sum_{n=0}^{N-1} \sum_k \omega_k \left(\hat{v}_{k,n}^\dagger \hat{v}_{k,n} + \frac{1}{2} \right), \quad (6)$$

where ω_k are the phonon frequencies, and $\hat{v}_{k,n}^\dagger$ and $\hat{v}_{k,n}$ are the k th phonon mode's creation and annihilation operators, respectively, for the n th molecule that satisfy the bosonic commutation relations. The last term \hat{H}_{SB} in Eq. (1) characterizes the system–bath interaction, which we assume takes the linear form

$$\hat{H}_{\text{SB}} = \sum_{n=0}^{N-1} \hat{\sigma}_n^\dagger \hat{\sigma}_n \sum_k c_k \left(\hat{v}_{k,n}^\dagger + \hat{v}_{k,n} \right), \quad (7)$$

where c_k denotes the coupling strength between the n th molecule and the k th phonon mode of its associated bath. To describe the interactions between the system and bath, we use the spectral density function,^{92,93}

$$J(\omega) = \pi \sum_k c_k^2 \delta(\omega - \omega_k). \quad (8)$$

We use a Drude–Lorentz form for the spectral density in our investigations,

$$J(\omega) = \frac{2\lambda\omega_v\omega}{\omega_v^2 + \omega^2}, \quad (9)$$

where ω_v is the bath characteristic frequency and the reorganization energy λ can be reformulated in terms of the coupling strength and the phonon frequencies as

$$\lambda = \frac{1}{\pi} \int_0^{+\infty} d\omega \frac{J(\omega)}{\omega} = \sum_k \frac{c_k^2}{\omega_k}. \quad (10)$$

Cavity loss is not considered in this work because our aim is to benchmark the influence of phonons on polariton relaxation dynamics. The influence of cavity loss can be easily modeled with Lindblad dynamics,^{52,94} or through stochastic Lindblad approaches.^{23,94}

B. Polariton states

We analyze \hat{H}_{S} in the single excitation subspace. The diabatic states (without considering the phonons) in the single excitation subspace are the photon-dressed ground state $|G, 1\rangle$ and the single-molecule excited state $|E_n, 0\rangle$. $|G, 1\rangle$ is defined as the state where all the molecules are in the ground state and one photon is in the cavity,

$$|G, 1\rangle = |g_0\rangle \otimes \cdots \otimes |g_n\rangle \cdots \otimes |g_{N-1}\rangle \otimes |1\rangle, \quad (11)$$

and $|E_n, 0\rangle$ is defined as the states where all the molecules are in the ground state except for the n th molecule,

$$|E_n, 0\rangle = |g_0\rangle \otimes \cdots \otimes |e_n\rangle \cdots \otimes |g_{N-1}\rangle \otimes |0\rangle. \quad (12)$$

In the single excitation manifold, we also have a collective “bright” excitonic state,

$$|B, 0\rangle = \frac{1}{\sqrt{N}} \sum_{n=0}^{N-1} |E_n, 0\rangle, \quad (13)$$

which couples to the $|G, 1\rangle$ state through \hat{H}_{LM} . This coupling leads to the polariton states $|\pm\rangle$, which are eigenstates of \hat{H}_{S} , expressed as follows:⁹¹

$$|+\rangle = \cos \theta |B, 0\rangle + \sin \theta |G, 1\rangle, \quad (14a)$$

$$|-\rangle = -\sin \theta |B, 0\rangle + \cos \theta |G, 1\rangle, \quad (14b)$$

where the mixing angle is

$$\theta = \frac{1}{2} \tan^{-1} \left[\frac{2\sqrt{N}g_c}{\omega_c - \omega_0 - \lambda} \right] \in [0, \frac{\pi}{2}), \quad (15)$$

and the corresponding energies ω_\pm of the $|\pm\rangle$ states are

$$\omega_\pm = \frac{\omega_0 + \lambda + \omega_c}{2} \pm \sqrt{Ng_c^2 + \frac{(\omega_0 + \lambda - \omega_c)^2}{4}}. \quad (16)$$

Furthermore, there exists $N - 1$ dark states $|\mathcal{D}_\alpha\rangle$, given by¹

$$|\mathcal{D}_\alpha\rangle = \sum_{n=0}^{N-1} C_{n,\alpha} |E_n, 0\rangle, \quad (17)$$

where the coefficients $C_{n,\alpha}$ satisfy

$$\frac{1}{\sqrt{N}} \sum_{n=0}^{N-1} C_{n,\alpha} = \langle B, 0 | \mathcal{D}_\alpha, 0 \rangle = 0. \quad (18)$$

We note from Eq. (18) that since the DS have no overlap with the collective “bright” states, they do not participate in the interaction with the cavity mode that is mediated by \hat{H}_{LM} . Furthermore, there is no optical transition from $|G, 0\rangle$ to $|\mathcal{D}_\alpha\rangle$; hence, it is optically dark. The choice of dark state is not unique. For example, one can express them as follows:^{91,95}

$$|\mathcal{D}_\alpha\rangle = \frac{1}{\sqrt{N}} \sum_{n=0}^{N-1} \exp \left(-2\pi i \frac{n\alpha}{N} \right) |E_n, 0\rangle, \quad (19)$$

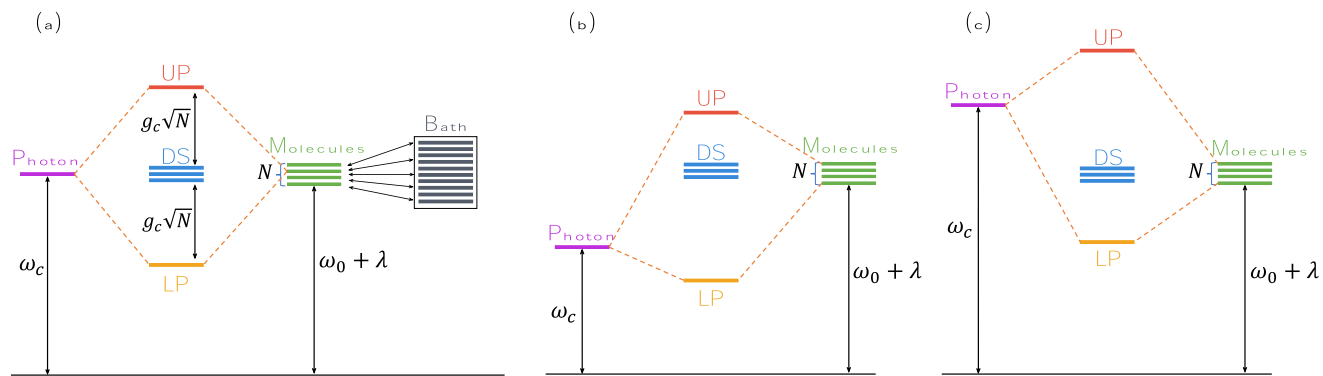


FIG. 1. Energy level diagrams of polariton states that are derived from the HTC Hamiltonian through hybridization of light and matter states. We show the relative positions of the DS with respect to the UP and the LP for three cases: (a) $\omega_c = \omega_0 + \lambda$ (zero detuning or resonance), (b) $\omega_c < \omega_0 + \lambda$ (negative detuning), and (c) $\omega_c > \omega_0 + \lambda$ (positive detuning).

where $\alpha \in \{0, \dots, N - 1\}$, which is fully delocalized among all N exciton states. Other choices are possible [see Eq. (8) in Ref. 96 for the Schur–Weyl basis].

The polariton states for the HTC model are outlined in Fig. 1. In the absence of exciton–phonon couplings, the $N - 1$ dark states are energetically degenerate and have the same energies as the excitation energy of the bare molecule plus the reorganization energy, as shown in Fig. 1(a). The UP and the LP in resonance are also energetically separated from the DS by an amount $\sqrt{N}g_c$ when the system is in resonance ($\omega_c = \omega_0 + \lambda$). However, when there is light–matter detuning (i.e., $\omega_c \neq \omega_0 + \lambda$), the DS are no longer separated in energy from the UP and the LP by the same amount. In particular, with negative light–matter detuning ($\omega_c < \omega_0 + \lambda$), the DS are closer in energy to the UP state, as illustrated in Fig. 1(b). On the other hand, with positive detuning ($\omega_c > \omega_0 + \lambda$), the DS are closer in energy to the LP state, as depicted in Fig. 1(c). Thus, the polariton relaxation dynamics, mediated by exciton–phonon coupling in \hat{H}_{SB} , will be affected by the energetics of the polariton and dark states due to different energy alignments caused by the light–matter detuning.

Note that the polariton state defined in Eq. (14) and the dark states in Eq. (17) are diabatic in nature because there is no nuclear configuration dependence. In this case, the exciton–phonon couplings \hat{H}_{SB} will couple these polariton states and make transitions among them.^{25,31} On the other hand, one can also choose to define $\hat{H}_{\text{S}} + \hat{H}_{\text{SB}}$ as the polariton Hamiltonian, whose eigenvector will be adiabatic polariton and dark states and both of their characters will parametrically depend on the nuclear configuration.²⁶ In this case, the phonon fluctuation caused by \hat{H}_{SB} on polariton and dark states will be counted as the adiabatic polariton energy fluctuations, and the transitions among these adiabatic polariton and dark states are caused by the nuclear kinetic energy operators (as the derivative couplings). This is the picture used in the theoretical simulations in Ref. 26 (see Fig. 4 in that reference). Nevertheless, rigorous quantum mechanical descriptions of the dynamics (for all DOF) will generate identical results in both pictures. Ehrenfest dynamics, as well as the mean-field-like approach (such as the mapping-based methods used in this work), are representation-

independent and thus generate identical results for both representations. The trajectory surface hopping approach, on the other hand, is not representation-independent and often performs the best in the adiabatic representation, so the adiabatic polariton Hamiltonian $\hat{H}_{\text{pl}} = \hat{H}_{\text{S}} + \hat{H}_{\text{SB}}$ should be used in these surface hopping simulations.

In the following, we briefly introduce the trajectory-based quantum dynamics approaches used in this work, which we treat

$$\hat{R}_{k,n} = \sqrt{\frac{\hbar}{2\omega_k}}(\hat{v}_{k,n}^\dagger + \hat{v}_{k,n}),$$

$$\hat{P}_{k,n} = i\sqrt{\frac{\hbar\omega_k}{2}}(\hat{v}_{k,n}^\dagger - \hat{v}_{k,n}),$$

inside the $\hat{h}_B + \hat{H}_{\text{SB}}$ as the classical DOF, and we describe the polariton quantum subsystem in the diabatic basis of $\{|G, 1\rangle, |E_n, 0\rangle\}$ for Ehrenfest dynamics, γ -SQC, spin-LSC, and spin-PLDM approaches. For the surface hopping method, the adiabatic polariton and dark states (see Ref. 26) are required, which are defined as the eigenstates of $\hat{H}_{\text{pl}} = \hat{H}_{\text{S}} + \hat{H}_{\text{SB}}$ as follows:

$$\hat{H}_{\text{pl}}(\mathbf{R})|\Psi(\mathbf{R})\rangle = \mathcal{E}(\mathbf{R})|\Psi(\mathbf{R})\rangle.$$

A schematic illustration of the adiabatic polariton energy (and dark energy) can be found in Fig. 4 in Ref. 26. Note that for a large N in the single excitation subspace, diagonalizing the above-mentioned equation is the computational bottleneck.

C. Non-adiabatic mapping dynamics methods

In this section, we briefly discuss the mapping-based quantum dynamics approaches used in this work. The details of the standard Ehrenfest dynamics and surface hopping approaches are provided in the [supplementary material](#). The common starting point of these mapping dynamics is the Meyer–Miller–Stock–Thoss (MMST) formalism,^{55,65,66} which maps the discrete quantum DOF (described as discrete states) onto continuous phase space variables. A Hamiltonian that contains a total of \mathcal{N} quantum states in the

diabatic representation $\{|a\rangle\}$ is expressed as

$$\hat{H} = \frac{1}{2M}\hat{\mathbf{P}}^2 + U_0(\hat{\mathbf{R}}), \quad (20)$$

$$+ \sum_a V_{aa}(\hat{\mathbf{R}})|a\rangle\langle a| + \frac{1}{2} \sum_{b \neq a} V_{ab}(\hat{\mathbf{R}})|a\rangle\langle b|, \quad (21)$$

where $\hat{\mathbf{R}}$ and $\hat{\mathbf{P}}$ are the position and momenta for the nuclear DOF, respectively, $U_0(\hat{\mathbf{R}})$ is the state-independent part of the Hamiltonian, and $V_{ab}(\hat{\mathbf{R}}) = \langle a|\hat{V}|b\rangle$. For the HTC model, we have

$$\hat{h}_B = \frac{1}{2M}\hat{\mathbf{P}}^2 + U_0(\hat{\mathbf{R}}), \quad (22a)$$

$$\hat{H}_S + \hat{H}_{SB} = \hat{V}. \quad (22b)$$

The MMST formalism maps the quantum Hamiltonian in Eq. (20) onto the following classical MMST Hamiltonian:

$$\mathcal{H}_m = \frac{1}{2M}\mathbf{P}^2 + \frac{1}{2} \sum_{ab} V_{ab}(\mathbf{R})(p_a p_b + q_a q_b - 2\gamma_b \delta_{ab}) + U_0(\mathbf{R}), \quad (23)$$

where $2\gamma_b$ is viewed as a parameter⁵⁶ that specifies the zero-point energy (ZPE) of the mapping oscillators.^{56,67,68,97} In principle, $2\gamma_b$ is state-specific and trajectory-specific.⁸⁵ The MMST mapping Hamiltonian has been historically justified by Stock and Thoss using the raising and lowering operators of a harmonic oscillator as the mapping operator.^{65,66} Recently, a more natural mapping has been derived using the $SU(N)$ Lie group theory or the so-called generalized spin mapping approach,⁶⁹ which is connected to the MMST mapping approach.^{68,69} In this work, we will focus on two recently developed mapping-based approaches: γ -SQC⁸⁵ and Spin-LSC.^{68,69} Both the approaches have been shown to significantly improve the accuracy of the population dynamics compared to the original MMST-based LSC-IVR approach,^{57,58} for nearly all model systems commonly tested in non-adiabatic simulations.⁵⁶ In addition, for many level system-bath-type models, LSC-IVR often generates negative population dynamics and gives less accurate results.⁹⁸ For this reason, we left the LSC-IVR approach in our comparison in this work and instead focus on the recently developed γ -SQC⁸⁵ and Spin-LSC.^{68,69} Note that there is recent progress in improving the accuracy of LSC-IVR, such as using the GQME approach⁷⁹ and the identity trick.⁹⁹ These approaches have been shown to provide a significant improvement in the accuracy dynamics of LSC-IVR for two-level systems,^{79,99} but extending them to many level systems is theoretically less straightforward.^{100,101}

Classical trajectories are generated based on Hamilton's equations of motion (EOM) for \mathcal{H}_m ,

$$\dot{q}_b = \partial \mathcal{H}_m / \partial p_b; \quad \dot{p}_a = -\partial \mathcal{H}_m / \partial q_a, \quad (24a)$$

$$\dot{\mathbf{R}} = \partial \mathcal{H}_m / \partial \mathbf{P}; \quad \dot{\mathbf{P}} = -\partial \mathcal{H}_m / \partial \mathbf{R} = \mathbf{F}, \quad (24b)$$

with the nuclear force expressed as

$$\mathbf{F} = -\frac{1}{2} \sum_{ab} \nabla U_{ab}(\mathbf{R})(p_a p_b + q_a q_b - 2\gamma_b \delta_{ab}) - \nabla U_0(\mathbf{R}). \quad (25)$$

The above-mentioned classical EOM for both mapping variables (for the quantum subsystem) and the classical DOF are propagated using the velocity Verlet algorithm.

1. The γ -SQC approach

The γ -SQC approach samples the initial electronic condition and estimates the population based on the action-angle variables, $\{\varepsilon_b, \theta_b\}$, expressed as follows:

$$\varepsilon_b = \frac{1}{2}(p_b^2 + q_b^2); \quad \theta_b = -\tan^{-1}\left(\frac{p_b}{q_b}\right). \quad (26)$$

They are inversely related to the mapping variables as follows:

$$q_b = \sqrt{2\varepsilon_b} \cos(\theta_b); \quad p_b = -\sqrt{2\varepsilon_b} \sin(\theta_b), \quad (27)$$

where ε_b is a positive-definite action variable that is directly proportional to the mapping variables' radius in action space.⁸⁵

The SQC approach calculates the population of electronic state $|b\rangle$, which will be evaluated as⁵⁶

$$\rho_{bb}(t) = \text{Tr}_{\mathbf{R}}\left[\hat{\rho}(0)e^{i\hat{H}t/\hbar}|b\rangle\langle b|e^{-i\hat{H}t/\hbar}\right] \approx \int d\tau \rho_W(\mathbf{P}, \mathbf{R}) W_a(\boldsymbol{\varepsilon}(0)) W_b(\boldsymbol{\varepsilon}(t)), \quad (28)$$

where $\hat{\rho}(0) = \hat{\rho}_{\mathbf{R}} \otimes |a\rangle\langle a|$ is the initial density operator, $\rho_W(\mathbf{P}, \mathbf{R})$ is the Wigner transform of the $\hat{\rho}_{\mathbf{R}}$ operator for the nuclear DOF, $\boldsymbol{\varepsilon} = \{\varepsilon_1, \varepsilon_2, \dots, \varepsilon_N\}$ is the positive-definite action variable vector for N electronic states,⁸⁵ $W_a(\boldsymbol{\varepsilon}) = \delta[\varepsilon_a - (1 + \gamma_a)] \prod_{a \neq b} \delta(\varepsilon_b - \gamma_b)$ is the Wigner transformed action variables,¹⁰² and $d\tau \equiv d\mathbf{P} \cdot d\mathbf{R} \cdot d\boldsymbol{\varepsilon} \cdot d\boldsymbol{\theta}$. For practical reasons, the delta functions above in $W_a(\boldsymbol{\varepsilon})$ are broadened using a distribution function (so-called window function) that is used to bin the resulting electronic action variables in action space.⁵⁶ Here, we used the triangle window,^{85,102} which is expressed as

$$W_b(\boldsymbol{\varepsilon}) = w_1(\varepsilon_b) \prod_{b' \neq b}^N w_0(\varepsilon_b, \varepsilon_{b'}), \quad (29)$$

where the window functions are defined as

$$w_1(\varepsilon) = \begin{cases} (2-\varepsilon)^{2-N}, & 1 < \varepsilon < 2, \\ 0, & \text{else,} \end{cases} \quad (30)$$

where N is the total number of states, and

$$w_0(\varepsilon, \varepsilon') = \begin{cases} 1, & \varepsilon' < 2 - \varepsilon, \\ 0, & \text{else,} \end{cases} \quad (31)$$

and trajectories are assigned to state b at time t if $\varepsilon_b \geq 1$ and $\varepsilon_{b'} < 1$ for all $b' \neq b$.

The time-dependent population of the state $|b\rangle$ is computed with Eq. (28). Using the window function estimator, the total population is no longer properly normalized due to the fraction of trajectories that are outside of any window region at any given time.⁶¹ Thus, the total population must be normalized⁶¹ with the following procedure:

$$\rho_{bb}(t)/\sum_{a=1}^N \rho_{aa}(t) \rightarrow \rho_{bb}(t). \quad (32)$$

In the γ -SQC approach,⁸⁵ it was proposed that the mapping ZPE should be chosen in such a way as to constrain the initial force to be composed purely of the initially occupied state.⁸⁵ The basic logic of γ -SQC is to choose a γ_b value for each state $|b\rangle$ in every given individual trajectory, such that the initial population is forced to respect the initial electronic excitation focused onto a single excited state. If the initial electronic state is $|a\rangle$, then

$$\gamma_b = \varepsilon_b - \delta_{ba}, \quad (33)$$

or equivalently,

$$\delta_{ba} = \varepsilon_b - \gamma_b, \quad (34)$$

where $\{\varepsilon_b\}$ are uniformly sampled inside the window function [Eq. (29)], and following that, the γ_b are chosen to satisfy Eq. (34).

These γ_b will be explicitly used in the EOMs in Eqs. (24) and (25), and in particular, the nuclear forces become

$$\mathbf{F} = -\frac{1}{2} \sum_{ab} \nabla V_{ab}(\mathbf{R}) (p_a p_b + q_a q_b - 2\gamma_b \delta_{ba}), \quad (35)$$

ensuring the initial forces (at $t = 0$) are simply $\mathbf{F} = -\nabla V_{aa}(\mathbf{R})$. Previously, without any adjustments to γ_b , the chosen values for γ_b were only dependent on the windowing function itself, i.e., $\gamma_b = 0.366$ for the square windows and $\gamma_b = 1/3$ for the triangle windows. With the above-mentioned γ -correction method,⁸⁵ each individual trajectory will have its own state-specific γ_b for state $|b\rangle$ that is completely independent of the choice of the window function. This method has been proven to provide very accurate non-adiabatic dynamics in model photo-dissociation problems (coupled Morse potential) and has outperformed fewest-switches surface hopping (FSSH) with decoherence correction in *ab initio* on-the-fly simulations.^{75,76}

2. The spin-LSC method

For the spin-LSC approach,^{67,68} one chooses a universal ZPE parameter $2\gamma_b = \Gamma$ for all states and trajectories. The spin-LSC population dynamics is calculated as

$$\begin{aligned} \rho_{bb}(t) &= \text{Tr}_{\mathbf{R}} [\hat{\rho}_{\mathbf{R}} \otimes |a\rangle\langle a| e^{i\hat{H}_t/\hbar} |b\rangle\langle b| e^{-i\hat{H}_t/\hbar}] \\ &\approx \int d\tau \rho_{\mathbf{W}}(\mathbf{P}, \mathbf{R}) [|a\rangle\langle a|_s(0) \cdot [|b\rangle\langle b|]_{\tilde{s}}(t)], \end{aligned} \quad (36)$$

where the population estimators are obtained from the Stratonovich–Weyl transformed electronic projection operators, with the expressions as follows:⁶⁸

$$[|a\rangle\langle a|_s] = \frac{1}{2} (q_a^2 + p_a^2 - \Gamma), \quad (37a)$$

$$[|b\rangle\langle b|]_{\tilde{s}} = \frac{\mathcal{N} + 1}{2(1 + \frac{\mathcal{N}\Gamma}{2})^2} \cdot (q_b^2 + p_b^2) - \frac{1 - \frac{\Gamma}{2}}{1 + \frac{\mathcal{N}\Gamma}{2}}, \quad (37b)$$

where \mathcal{N} is the total number of states. The parameter Γ is related to the radius of the generalized Bloch sphere r_s through $\Gamma = \frac{2}{\mathcal{N}}(r_s - 1)$, where s and \tilde{s} are complementary indices in the Stratonovich–Weyl transform. Among the vast parameter space, one of the best-performing choices^{67,68} is when $r_s = r_{\tilde{s}} = \sqrt{\mathcal{N} + 1}$, which is referred to as $s = W$, leading to a ZPE parameter,

$$\Gamma = \frac{2}{\mathcal{N}} (\sqrt{\mathcal{N} + 1} - 1) \quad (38)$$

as well as the identical expression of $[|a\rangle\langle a|_s]$ and $[|b\rangle\langle b|]_{\tilde{s}}$ in Eq. (37). We further use the focused initial condition^{67,68} that replaces the sampling of the mapping variables in the $d\tau$ integral of Eq. (36) with specific values of the mapping variables, such that $\frac{1}{2}(q_a^2 + p_a^2 - \Gamma) = 1$ for initially occupied state $|a\rangle$ and $\frac{1}{2}(q_b^2 + p_b^2 - \Gamma) = 0$ for the initially unoccupied states $|b\rangle$. The angle variables $\{\theta_b\}$ [Eq. (26)] are randomly sampled⁶⁸ in the range of $[0, 2\pi]$. More computational details for the γ -SQC and spin-LSC are provided in Sec. III B.

III. COMPUTATIONAL DETAILS

A. Initial conditions

We describe the details of the HTC models used in our benchmark and the corresponding initial condition for the dynamics. The initial condition for all our simulations is assumed to be separable, and hence, the density matrix $\hat{\rho}$ is given by

$$\hat{\rho} = \hat{\rho}_S \otimes \frac{e^{-\beta \hat{h}_B}}{\mathcal{Z}_B}, \quad (39)$$

TABLE I. Parameters assigned in different models used in this work. The results from model 1 to model 4 are presented in the main text, while the results of model 5 and model 6 are presented in the supplementary material.

Model	N	$\omega_c - \omega_0 - \lambda$ (meV)	g_c (meV)	λ (meV)	ω_v (meV)	β (a.u.)
1	5/10/15	0	68.1	30	24.8	1000
2	10	-200/0/200	68.1	30	24.8	1000
3	10	0	40.8/68.1/96.1	30	24.8	1000
4	10	0	68.1	10/30/50	24.8	1000
5	10	0	68.1	30	12.4/24.8/37.2	1000
6	10	0	68.1	30	24.8	250/1000/4000

where $\hat{\rho}_S$ is the system-reduced density operator, $\beta = 1/k_B T$ is the inverse temperature, and $\mathcal{Z}_B = \text{Tr}[e^{-\beta h_B}]$ is the bare-bath partition function. In Eq. (39), we assume that the bath is in thermal equilibrium so that the bath-reduced density matrix operator takes the form of a Boltzmann distribution. In addition, the system is initially placed in the UP state $|\Psi(0)\rangle = |+\rangle$ and the associated system reduced density operator is given by $\hat{\rho}_S = |+\rangle\langle+|$. This initial state is chosen so that we can observe the relaxation from the UP to the DS and LP state because of exciton–phonon coupling.

B. Model parameters

We construct six HTC benchmark models to investigate the performance of the trajectory-based non-adiabatic methods to simulate polariton relaxation dynamics. These models scan a range of the following physical parameters: (1) number of molecules (N), (2) light–matter detuning ($\omega_c - \omega_0 - \lambda$), (3) single-molecule coupling strength (g_c), (4) reorganization energy (λ), (5) bath cutoff frequency (ω_v), and (6) temperature ($\beta = 1/k_B T$).

In each model, we vary one parameter and fix the other five parameters. The values of these parameters for all six models are provided in Table I. We note that by changing the parameters in

models 1–3, the polariton relaxation dynamics are affected through the system contribution to the Hamiltonian, while in changing the parameters in models 4–6, the dynamics are affected through the system–bath interaction term. Furthermore, the results for models 1–4 are presented in the main text in the following, while models 5 and 6 are provided in Sec. III of the [supplementary material](#).

C. Details on the HEOM simulations

For the model we considered, the molecular phonon bath is described by the Drude–Lorentz spectral density, so that the bare-bath time-correlation function (TCF) decomposition is achieved using the Padé spectral decomposition (PSD) scheme.^{103–105} Here, we use the $[N - 1/N]$ scheme¹⁰⁵ with 2 low-temperature correction terms. For HEOM propagation, we use the fourth-order Runge–Kutta (RK-4) integrator with a time step of 0.005 fs, together with the on-the-fly filtering algorithm¹⁰⁶ with an error tolerance of 1×10^{-6} . The number of tiers (i.e., hierarchical expansion of the EOM) is set as 20. The convergence of the calculation is carefully checked with the above-mentioned parameters. In addition, a factorizable initial full-density matrix is applied, which is the same as

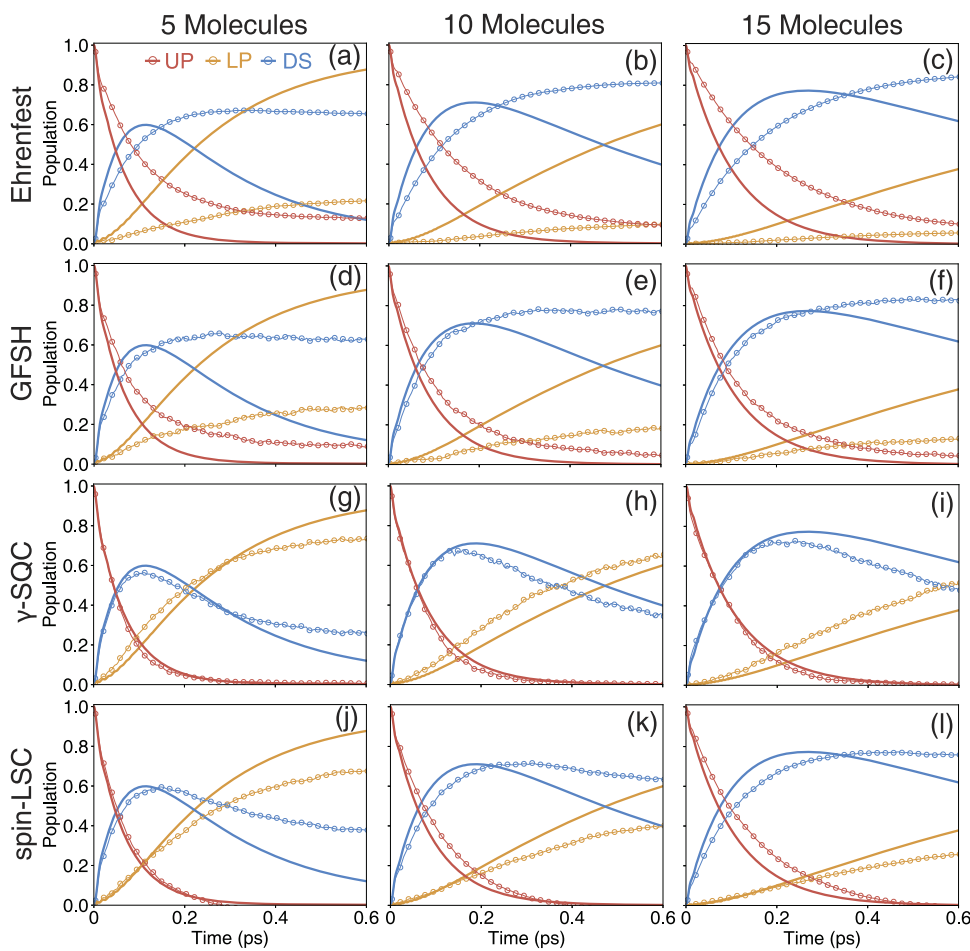


FIG. 2. Population dynamics of the UP and the LP states, and sum over all dark states for the HTC model computed with different MQC dynamics methods, including Ehrenfest, GFSH, γ -SQC, and spin-LSC. Different numbers of molecules ($N = 5/10/15$) are used in the dynamics simulations. The cavity frequency is $\omega_c = 2.0$ eV, the light–matter coupling strength is $g_c = 68.1$ meV, the reorganization energy is $\lambda = 30$ meV, the temperature is $\beta = 1000$ a.u., and the cutoff frequency during the initial sampling process is $\omega_v = 24.8$ meV. See model 1 in Table I.

Eq. (39). The details about the HEOM method are provided in Sec. I of the [supplementary material](#).

D. Details of the trajectory-based dynamics

To perform the γ -SQC dynamics, we need to sample the initial condition for the quantum subsystem. In this work, we sample the action-angle variables $\{\varepsilon_b, \theta_b\}$ and subsequently transform them to the mapping variables $\{p_b, q_b\}$ using Eq. (27). The action variables $\{\varepsilon_b\}$ are sampled according to the window function in Eq. (29), and the angle variables $\{\theta_b\}$ are randomly sampled from $[0, 2\pi]$. The triangle window is used in this work, although the square window generates similar results.

For the spin-LSC dynamics, we use the focused initial conditions⁶⁸ described in Sec. II C, where the action variable ε_a is set to be $1 + \Gamma/2$ for the initially occupied state and $\Gamma/2$ for the initially unoccupied state, with Γ expressed in Eq. (38). The angle variables $\{\theta_b\}$ are randomly generated between $[0, 2\pi]$ as in the γ -SQC method. The canonical mapping variables are obtained from Eq. (27).

The initial nuclear distribution of all trajectory-based simulations (Ehrenfest, GFSH, γ -SQC, and spin-LSC) are generated by sampling the Wigner density,

$$[\langle R|\chi \rangle]_w = \frac{1}{\hbar\pi} e^{-M(P^2 + \omega_0^2(R - R_0)^2)/\omega_0\hbar}, \quad (40)$$

which is the Wigner transformation of the nuclear wavefunction $\chi(R) = \langle R|\chi \rangle$ in the initial state. Here, R and P are the nuclear coordinate and momentum, respectively. The nuclear time step used in all the trajectory-based simulations is $dt = 3.0$ a.u., with 200 equally spaced time steps for the mapping variables' integration during each nuclear time step. The equations of motion in Eqs. (24) and (25) are integrated using a second-order symplectic integrator for the MMST variables.^{107,108} The population dynamics using all trajectory-based methods were averaged over 10 000 trajectories. Note that the results from SH and γ -SQC are less smooth compared to the other trajectory-based method due to their active state estimator and the window estimator, respectively. Furthermore, when the total number of states $N + 1$ increases, the number of trajectories in a given population window in the SQC-approach

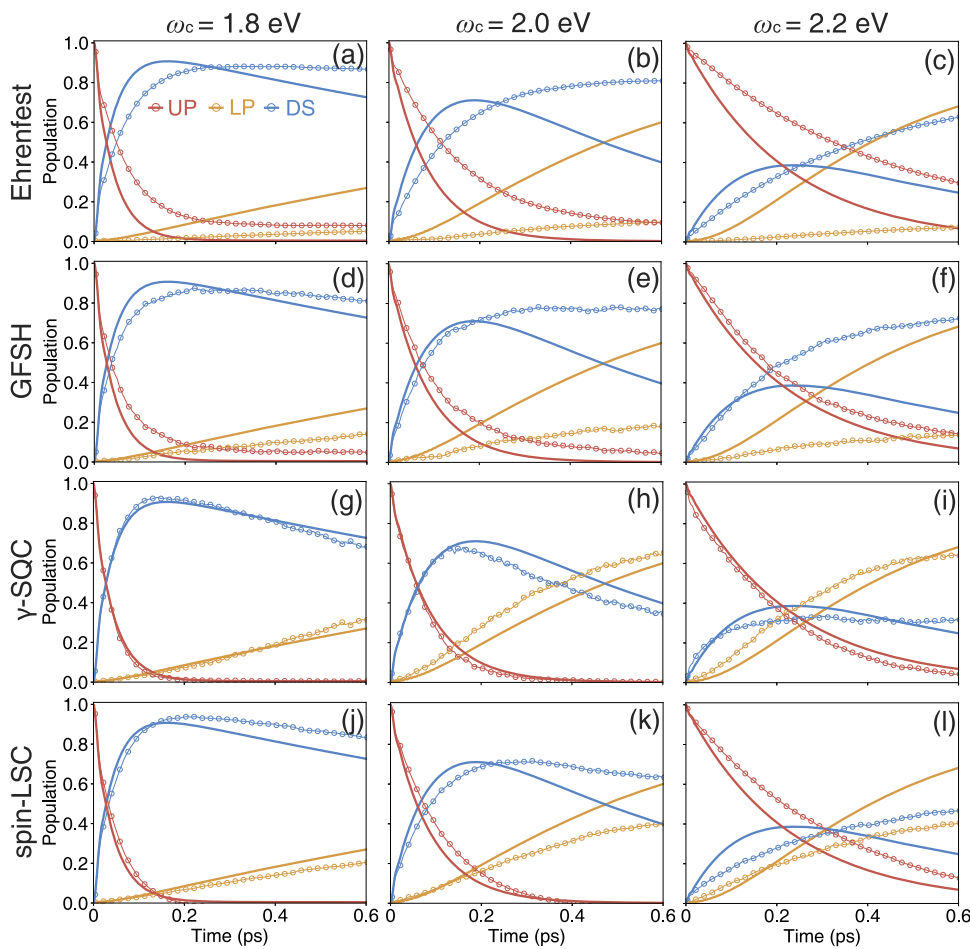


FIG. 3. Population dynamics of the UP and the LP states, and sum over all dark states for the HTC model computed with different MQC dynamics methods, including Ehrenfest, GFSH, γ -SQC, and spin-LSC. Different cavity frequencies ($\omega_c = 1.8, 2.0, 2.2$ eV) are used in the dynamics simulations. The number of molecules is $N = 10$; the light-matter coupling strength is $g_c = 68.1$ meV; and the reorganization energy is $\lambda = 30$ meV. See model 2 in [Table I](#) for details.

gradually decrease in time,¹⁰⁹ resulting in less smooth population estimation.

IV. RESULTS

We present the population dynamics of the polariton states and dark states for models 1–4 in this section. Figure 2 shows the dynamics for model 1, which varies the number of molecules N from five molecules to 15 molecules; Fig. 3 presents the dynamics for model 2, where the light-matter detuning $\omega_c - \omega_0 - \lambda$ varies from negative to positive values; Fig. 4 illustrates the population dynamics for model 3, which varies the single-molecule coupling strength g_c from 40.8 to 96.1 meV; and Fig. 5 depicts the population dynamics for model 4, where the reorganization energy λ is varied from 10 to 50 meV. The trajectory-based methods are depicted using open circles and are compared to numerically exact results (HEOM) depicted using solid lines.

We see from Figs. 2–5 that all trajectory-based methods are able to semi-quantitatively account for the relaxation of the UP state to the DS and eventually to the LP state. However, both MQC methods (Ehrenfest and GFSH) predict a slower relaxation rate and a larger steady-state population [see Figs. 2(a)–2(f), 3(a)–3(f), 4(a)–4(f), and

5(a)–5(f)] for the UP state compared to the HEOM result. Focusing on the transitions into and out of the dark states, we observe that both MQC methods are only able to capture the increase in the total dark state populations qualitatively. After the dark state populations have reached a maximum value, both MQC methods predict little changes in the dark state population, which is in contrast to numerically exact results from HEOM simulation. As a result, the increase in the LP population calculated from both MQC methods, which comes from the transitions from the dark states, is smaller than that predicted by using the HEOM method. One exception to these observations about the dark states is given in Fig. 3(d), where the GFSH method predicts comparable dark state populations compared to the HEOM method for negative detuning ($\omega_c - \omega_0 - \lambda = -200$ meV).

In contrast, the mapping-based methods (γ -SQC and spin-LSC) show more accurate relaxation dynamics from the UP state, compared to the HEOM results, and the steady-state population for the UP is also similar to the exact HEOM dynamics [see Figs. 2(g)–2(l), 3(g)–3(l), 4(g)–4(l), and 5(g)–5(l)]. We also observe that the transitions to the dark states are better captured with these mapping-based methods, although the γ -SQC method outperforms the spin-LSC method in predicting the longer time transitions from

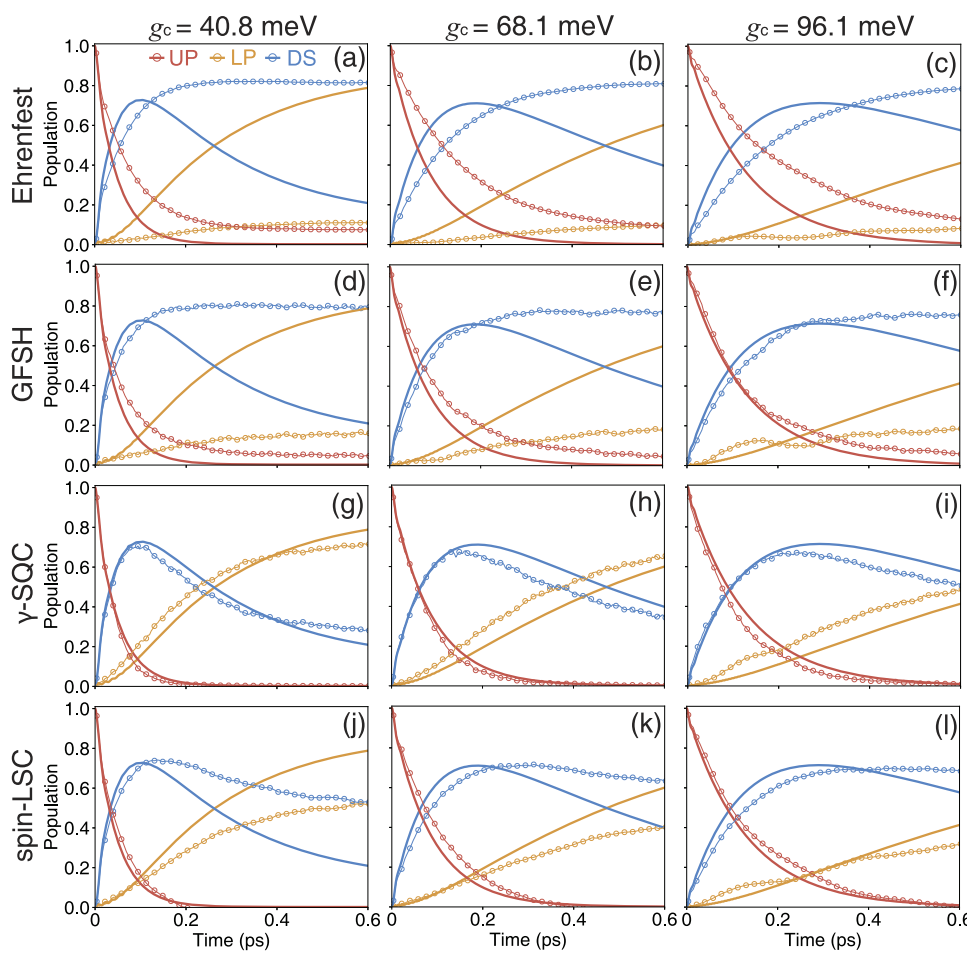


FIG. 4. Population dynamics of the UP and the LP states, and sum over all dark states for the HTC model computed with different MQC dynamics methods, including Ehrenfest, GFSH, γ -SQC, and spin-LSC. Different light-matter coupling strengths ($g_c = 40.8/68.1/96.1$ meV) are used in the dynamics simulations. The number of molecules is $N = 10$; the cavity frequency is $\omega_c = 2.0$ eV; and the reorganization energy is $\lambda = 30$ meV. See model 3 in Table I for details.

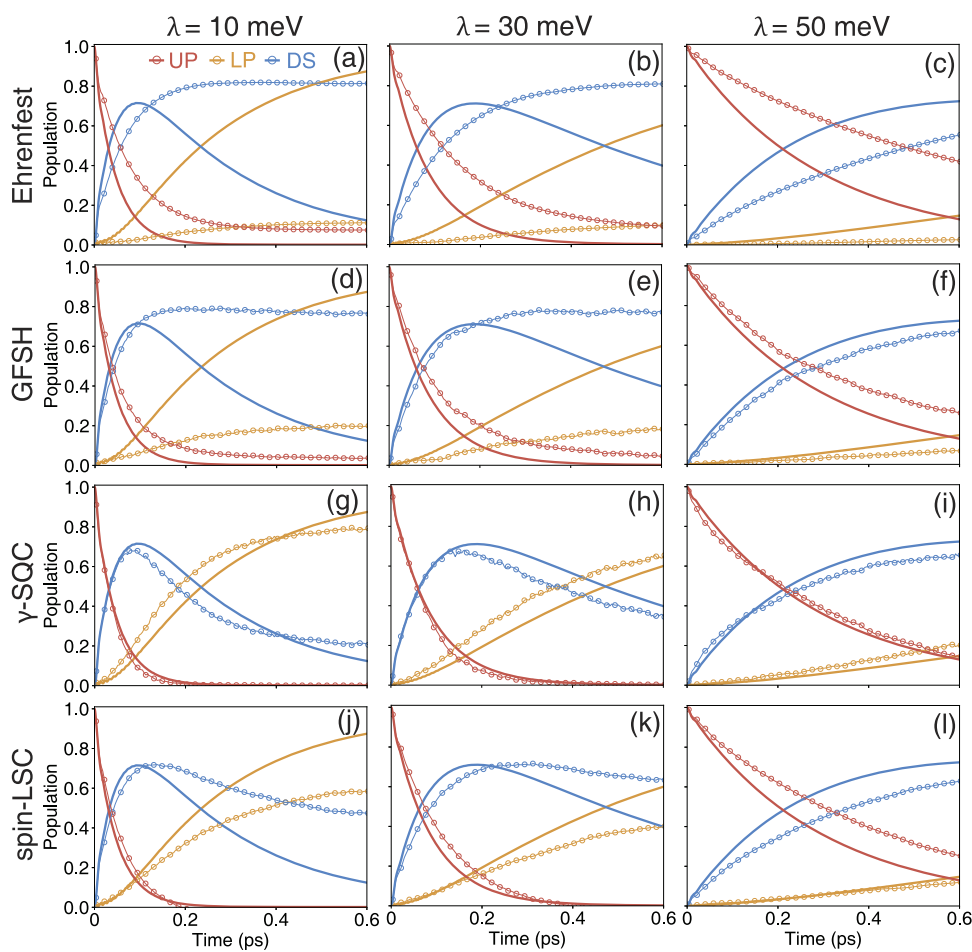


FIG. 5. Population dynamics of the UP and the LP states, and sum over all DS for the HTC model computed with different MQC dynamics methods, including Ehrenfest, GFSH, γ -SQC, and spin-LSC. Different reorganization energy ($\lambda = 10/30/50$ meV) are used in the dynamics simulations. The number of molecules is $N = 10$, and the cavity frequency is $\omega_c = 2.0$ eV. See model 4 in Table I for details.

the dark states to the LP state. Furthermore, the population of the LP state computed from the mapping-based method is comparable with the populations of the LP state predicted from the HEOM method. In addition, we note that for the population of the LP state, the γ -SQC method tends to overestimate the population compared to the HEOM method while the spin-LSC method tends to underestimate the population compared to the HEOM method [see Figs. 4(h) and 4(k) for an example].

Further benchmark results for model 5 and model 6 are provided in the [supplementary material](#), with changing bath characteristic frequency ω_v (Fig. S1 for model 5) and temperature T (Fig. S2 for model 6). All the methods show qualitatively correct dynamics; the mapping methods are more accurate than the MQC approaches; and γ -SQC slightly outperforms spin-LSC.

Finally, in Fig. 6, we present a further comparison of the polariton relaxation dynamics computed using the spin-PLDM approach^{70,71} for model 1. The theoretical details of this approach can be found in Ref. 70. Similar to the original PLDM approach,^{59,60} spin-PLDM explicitly accounts for the forward and backward propagators of the quantum subsystem, using the forward and backward mapping variables. One can see in Fig. 6 that spin-PLDM provides more accurate results compared to spin-LSC and achieves accuracy at a similar level of γ -SQC [see Figs. 2(g) and 2(h)]. However, being

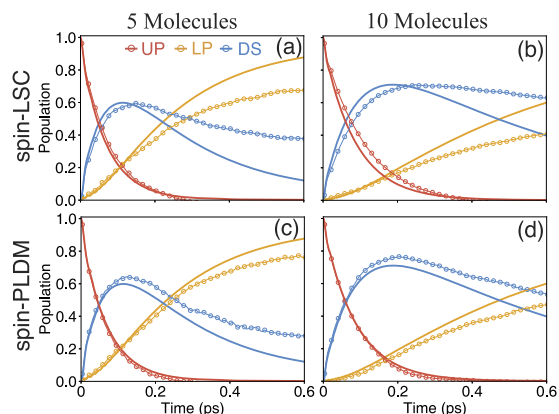


FIG. 6. Same as Fig. 2, by comparing results obtained from spin-LSC and spin-PLDM.

a partially forward and backward method, the computational cost of spin-PLDM is significantly increased compared to the Ehrenfest method and all linearized mapping approaches (γ -SQC and spin-LSC).

V. CONCLUSIONS

In this paper, we provide several benchmark results for various trajectory-based non-adiabatic simulations on polariton relaxation dynamics. The non-adiabatic methods that we use in our benchmark are well-known in the literature, such as MQC-based methods and the recently developed mapping-based methods (both γ -SQC and spin-mapping representation). In particular, we showed that the MQC-based methods (MFE and GFSH) are able to qualitatively capture the initial relaxation dynamics of the polaritonic system but are unable to accurately describe subsequent relaxation to the DS and the LP state. In comparison with the other methods, we find that the γ -SQC method is able to accurately capture all relevant relaxation dynamics of the polariton system, including the transition from the DS to the LP state at long time scales. The spin-mapping method that we chose (spin-LSC) also markedly improves on the MQC-based methods in terms of simulating the relaxation dynamics of polaritons, although it is less accurate compared to SQC when describing the correct rates of relaxation from the DS to the LP state.

Thus, for the models investigated in this work, the γ -SQC method outperforms the other three methods to describe the relevant polariton physics in the HTC model. Despite this observation, more work remains to be done to theoretically investigate the limitations of the other trajectory-based methods and address their shortcomings in terms of simulating the relevant dynamics for polariton chemistry and physics. We further envision that our benchmark results will provide useful information to the emergent polariton chemistry and physics community by showcasing the applicability of various trajectory-based methods to analyze problems of interest, such as polariton photochemical processes and polariton transport dynamics.^{17,20,110,111}

We have simulated the polariton relaxation dynamics in six different model systems by systematically changing the numbers of molecules N , light-matter detunings, Rabi splitting, phonon reorganization energy, phonon frequency, and temperature. The insights obtained from all simulations are that the relaxation dynamics are sensitive to the parameters we scanned. From the Hamiltonian, the phonon coupling is the main source mediating the relaxation of the UP to DS and eventually to the LP state. In our previous work,²⁵ we have rigorously derived rate theory based on the equilibrium and non-equilibrium golden rule, which provides a semi-quantitative description of the polariton relaxation dynamics. For the simplest Fermi's Golden rule (FGR) [see Eq. (30) in Ref. 25], one can indeed see how these quantities influence the relaxation dynamics. These simple expressions not only provide reliable population dynamics²⁵ but also helped understand the behavior of line shape as detuning³⁰ and the polariton decoherence dynamics.³¹ The current work, through scanning various parameters, confirms these early observations of relaxation dynamics interpreted from the FGR. On the other hand, we want to emphasize that the focus of the current work is to assess the numerical behavior of the trajectory-based method.

As we approach the large N limit with $N \sim 10^6$, which is considered to be the experimentally relevant regime,^{1,2} we note that one should take advantage of the well-known mean-field solution^{112,113} or the recently proposed CUT-E approach^{114,115} (for the zero-temperature case and with a single high-frequency vibration mode

per molecule) that effectively only treats one or a few molecules. We can also exploit the sparsity of the HTC Hamiltonian²⁴ to enable direct simulations of $N \sim 10^6$ molecules coupled to a single cavity mode in the single excitation subspace with trajectory-based methods. One could also explore the relatively short memory kernel time compared to the density matrix dynamics time to facilitate the simulations.^{79,116} These directions remain to be explored in the future.

SUPPLEMENTARY MATERIAL

See the [supplementary material](#) for details about the HEOM method, the Ehrenfest dynamics, the Global Flux Surface Hopping non-adiabatic methods used to perform the benchmark simulations, and polariton relaxation dynamics for models 5 and 6.

ACKNOWLEDGMENTS

This work was supported by the National Science Foundation Award under Grant Nos. CHE-2244683 and OAC-2311442. D.H. is supported by the National Science Fund of China (Grant No. 22403008), the Beijing Natural Science Foundation (Grant No. 2244074), and the start-up funding (Grant No. 312200502511) from the Beijing Normal University at Zhuhai. W.Y. acknowledges the support of the Moses Passer Graduate Fellowship at the University of Rochester. P.H. acknowledges the support of the Cottrell Scholar Award (a program by the Research Corporation for Science Advancement). Computing resources were provided by the Center for Integrated Research Computing (CIRC) at the University of Rochester and by the Interdisciplinary Intelligence Super-Computer Center of the Beijing Normal University at Zhuhai. We thank Eric Koessler for valuable comments on the manuscript.

AUTHOR DECLARATIONS

Conflict of Interest

The authors have no conflicts to disclose.

Author Contributions

D.H. and B. X. K. C. contributed equally to this work.

Deping Hu: Conceptualization (equal); Data curation (lead); Formal analysis (equal); Funding acquisition (lead); Investigation (equal); Methodology (equal); Project administration (equal); Software (lead); Supervision (equal); Validation (lead); Visualization (equal); Writing – original draft (equal); Writing – review & editing (equal). **Benjamin X. K. Chng:** Conceptualization (equal); Data curation (equal); Formal analysis (equal); Investigation (equal); Methodology (equal); Validation (equal); Visualization (lead); Writing – original draft (lead); Writing – review & editing (equal). **Wenxiang Ying:** Conceptualization (equal); Data curation (supporting); Formal analysis (equal); Investigation (equal); Methodology (equal); Software (equal); Validation (equal); Writing – original draft (sup-

porting); Writing – review & editing (supporting). **Pengfei Huo:** Conceptualization (equal); Formal analysis (equal); Funding acquisition (lead); Investigation (equal); Methodology (equal); Project administration (equal); Supervision (equal); Writing – original draft (equal); Writing – review & editing (lead).

DATA AVAILABILITY

The data that support the findings of this study are available from the corresponding author upon a reasonable request.

REFERENCES

- ¹A. Mandal, M. A. D. Taylor, B. M. Weight, E. R. Koessler, X. Li, and P. Huo, “Theoretical advances in polariton chemistry and molecular cavity quantum electrodynamics,” *Chem. Rev.* **123**(16), 9786–9879 (2023).
- ²R. F. Ribeiro, L. A. Martínez-Martínez, M. Du, J. Campos Gonzalez-Angulo, and J. Yuen-Zhou, “Polariton chemistry: Controlling molecular dynamics with optical cavities,” *Chem. Sci.* **9**(30), 6325–6339 (2018).
- ³J. Feist, J. Galego, and F. J. García-Vidal, “Polaritonic chemistry with organic molecules,” *ACS Photonics* **5**, 205–216 (2018).
- ⁴A. Mandal and P. Huo, “Investigating new reactivities enabled by polariton photochemistry,” *J. Phys. Chem. Lett.* **10**(18), 5519–5529 (2019).
- ⁵H. L. Luk, J. Feist, J. J. Toppari, and G. Groenhof, “Multiscale molecular dynamics simulations of polaritonic chemistry,” *J. Chem. Theory Comput.* **13**, 4324–4335 (2017).
- ⁶G. Groenhof and J. J. Toppari, “Coherent light harvesting through strong coupling to confined light,” *J. Phys. Chem. Lett.* **9**, 4848–4851 (2018).
- ⁷G. Groenhof, C. Climent, J. Feist, D. Morozov, and J. J. Toppari, “Tracking polariton relaxation with multiscale molecular dynamics simulations,” *J. Phys. Chem. Lett.* **10**, 5476–5483 (2019).
- ⁸R. H. Tichauer, J. Feist, and G. Groenhof, “Multi-scale dynamics simulations of molecular polaritons: The effect of multiple cavity modes on polariton relaxation,” *J. Chem. Phys.* **154**(10), 104112 (2021).
- ⁹T. W. Ebbesen, “Hybrid light-matter states in a molecular and material science perspective,” *Acc. Chem. Res.* **49**(11), 2403–2412 (2016).
- ¹⁰M. Kowalewski and S. Mukamel, “Manipulating molecules with quantum light,” *Proc. Natl. Acad. Sci. U. S. A.* **114**(13), 3278–3280 (2017).
- ¹¹J. Flick, M. Ruggenthaler, H. Appel, and A. Rubio, “Atoms and molecules in cavities, from weak to strong coupling in quantum-electrodynamics (QED) chemistry,” *Proc. Natl. Acad. Sci. U. S. A.* **114**, 3026–3034 (2017).
- ¹²J. A. Hutchison, T. Schwartz, C. Genet, E. Devaux, and T. W. Ebbesen, “Modifying chemical landscapes by coupling to vacuum fields,” *Angew. Chem., Int. Ed.* **51**, 1592–1596 (2012).
- ¹³A. Thomas, L. Lethuillier-Karl, K. Nagarajan, R. M. A. Vergauwe, J. George, T. Chervy, A. Shalabney, E. Devaux, C. Genet, J. Moran, and T. W. Ebbesen, “Tilting a ground-state reactivity landscape by vibrational strong coupling,” *Science* **363**(6427), 615–619 (2019).
- ¹⁴A. Mandal, T. D. Krauss, and P. Huo, “Polariton-mediated electron transfer via cavity quantum electrodynamics,” *J. Phys. Chem. B* **124**(29), 6321–6340 (2020).
- ¹⁵M. Balasubrahmanyam, A. Simkovich, A. Golombok, G. Sandik, G. Ankonina, and T. Schwartz, “From enhanced diffusion to ultrafast ballistic motion of hybrid light-matter excitations,” *Nat. Mater.* **22**(3), 338–344 (2023).
- ¹⁶R. Pandya, A. Ashoka, K. Georgiou, J. Sung, R. Jayaprakash, S. Renken, L. Gai, Z. Shen, A. Rao, and A. J. Musser, “Tuning the coherent propagation of organic exciton-polaritons through dark state delocalization,” *Adv. Sci.* **9**(18), 2105569 (2022).
- ¹⁷D. Xu, A. Mandal, J. M. Baxter, S.-W. Cheng, I. Lee, H. Su, S. Liu, D. R. Reichman, and M. Delor, “Ultrafast imaging of polariton propagation and interactions,” *Nat. Commun.* **14**(1), 3881 (2023).
- ¹⁸B. Liu, X. Huang, S. Hou, D. Fan, and S. R. Forrest, “Photocurrent generation following long-range propagation of organic exciton-polaritons,” *Optica* **9**(9), 1029–1036 (2022).
- ¹⁹B. Liu, J. Lynch, H. Zhao, B. R. Conran, C. McAleese, D. Jariwala, and S. R. Forrest, “Long-range propagation of exciton-polaritons in large-area 2D semiconductor monolayers,” *ACS Nano* **17**(15), 14442–14448 (2023).
- ²⁰B. X. K. Chng, M. E. Mondal, W. Ying, and P. Huo, “Quantum dynamics simulations of exciton polariton transport,” *Nano Lett.* **25**(4), 1617–1622 (2025).
- ²¹F. Herrera and F. C. Spano, “Cavity-controlled chemistry in molecular ensembles,” *Phys. Rev. Lett.* **116**(23), 238301 (2016).
- ²²F. Herrera and F. C. Spano, “Theory of nanoscale organic cavities: The essential role of vibration-photon dressed states,” *ACS Photonics* **5**(1), 65–79 (2018).
- ²³M. E. Mondal, E. R. Koessler, J. Provazza, A. N. Vamivakas, S. T. Cundiff, T. D. Krauss, and P. Huo, “Quantum dynamics simulations of the 2D spectroscopy for exciton polaritons,” *J. Chem. Phys.* **159**(9), 094102 (2023).
- ²⁴M. E. Mondal, A. N. Vamivakas, S. T. Cundiff, T. D. Krauss, and P. Huo, “Polariton spectra under the collective coupling regime. I. Efficient simulation of linear spectra and quantum dynamics,” *J. Chem. Phys.* **162**(1), 014114 (2025).
- ²⁵Y. Lai, W. Ying, and P. Huo, “Non-equilibrium rate theory for polariton relaxation dynamics,” *J. Chem. Phys.* **161**, 104109 (2024).
- ²⁶L. Qiu, A. Mandal, O. Morshed, M. T. Meidenbauer, W. Girten, P. Huo, A. N. Vamivakas, and T. D. Krauss, “Molecular polaritons generated from strong coupling between CdSe nanoplatelets and a dielectric optical cavity,” *J. Phys. Chem. Lett.* **12**(20), 5030–5038 (2021).
- ²⁷M. Amin, E. R. Koessler, O. Morshed, F. Awan, N. M. B. Cogan, R. Collison, T. M. Tumiel, W. Girten, C. S. Leiter, A. N. Vamivakas, P. Huo, and T. D. Krauss, “Cavity controlled upconversion in CdSe nanoplatelet polaritons,” *ACS Nano* **18**(32), 21388–21398 (2024).
- ²⁸O. Morshed, M. Amin, N. M. B. Cogan, E. R. Koessler, R. Collison, T. M. Tumiel, W. Girten, F. Awan, L. Mathis, P. Huo *et al.*, “Room-temperature strong coupling between CdSe nanoplatelets and a metal-DBR Fabry-Pérot cavity,” *J. Chem. Phys.* **161**(1), 014710 (2024).
- ²⁹F. Freire-Fernández, N. G. Sinai, M. J. Hui Tan, S. M. Park, E. R. Koessler, T. Krauss, P. Huo, and T. W. Odom, “Room-temperature polariton lasing from CdSe core-only nanoplatelets,” *ACS Nano* **18**, 15177–15184 (2024).
- ³⁰W. Ying, M. E. Mondal, and P. Huo, “Theory and quantum dynamics simulations of exciton-polariton motional narrowing,” *J. Chem. Phys.* **161**(6), 064105 (2024).
- ³¹B. X. K. Chng, W. Ying, Y. Lai, A. N. Vamivakas, S. T. Cundiff, T. D. Krauss, and P. Huo, “Mechanism of molecular polariton decoherence in the collective light-matter couplings regime,” *J. Phys. Chem. Lett.* **15**, 11773–11783 (2024).
- ³²J. Galego, F. J. García-Vidal, and J. Feist, “Cavity-induced modifications of molecular structure in the strong-coupling regime,” *Phys. Rev. X* **5**(4), 041022 (2015).
- ³³D. Sanvitto and S. Kéna-Cohen, “The road towards polaritonic devices,” *Nat. Mater.* **15**(10), 1061–1073 (2016).
- ³⁴A. M. Berghuis, R. H. Tichauer, L. M. A. de Jong, I. Sokolovskii, P. Bai, M. Ramezani, S. Murai, G. Groenhof, and J. Gómez Rivas, “Controlling exciton propagation in organic crystals through strong coupling to plasmonic nanoparticle arrays,” *ACS Photonics* **9**(7), 2263–2272 (2022).
- ³⁵S. Baieva, O. Hakamaa, G. Groenhof, T. T. Heikkilä, and J. J. Toppari, “Dynamics of strongly coupled modes between surface plasmon polaritons and photoactive molecules: The effect of the Stokes shift,” *ACS Photonics* **4**(1), 28–37 (2017).
- ³⁶R. H. Tichauer, D. Morozov, I. Sokolovskii, J. J. Toppari, and G. Groenhof, “Identifying vibrations that control non-adiabatic relaxation of polaritons in strongly coupled molecule-cavity systems,” *J. Phys. Chem. Lett.* **13**(27), 6259–6267 (2022).
- ³⁷K. B. Arnardottir, A. J. Moilanen, A. Strashko, P. Törmä, and J. Keeling, “Multimode organic polariton lasing,” *Phys. Rev. Lett.* **125**(23), 233603 (2020).
- ³⁸S. Takahashi and K. Watanabe, “Decoupling from a thermal bath via molecular polariton formation,” *J. Phys. Chem. Lett.* **11**(4), 1349–1356 (2020).
- ³⁹J. C. Tully, “Perspective: Nonadiabatic dynamics theory,” *J. Chem. Phys.* **137**(22), 22A301 (2012).
- ⁴⁰M. Barbatti, “Nonadiabatic dynamics with trajectory surface hopping method,” *WIREs Comput. Mol. Sci.* **1**, 620–633 (2011).

- ⁴¹S. Mai, P. Marquetand, and L. Gonzalez, "A general method to describe inter-system crossing dynamics in trajectory surface hopping," *Int. J. Quantum Chem.* **115**, 1215–1231 (2015).
- ⁴²D. Hu, W. Ying, and P. Huo, "Resonance enhancement of vibrational polariton chemistry obtained from the mixed quantum-classical dynamics simulations," *J. Phys. Chem. Lett.* **14**(49), 11208–11216 (2023).
- ⁴³G. Kåb, "Mean field Ehrenfest quantum/classical simulation of vibrational energy relaxation in a simple liquid," *Phys. Rev. E* **66**(4), 046117 (2002).
- ⁴⁴J. C. Tully, "Molecular dynamics with electronic transitions," *J. Chem. Phys.* **93**(2), 1061–1071 (1990).
- ⁴⁵S. Hammes-Schiffer and J. C. Tully, "Proton transfer in solution: Molecular dynamics with quantum transitions," *J. Chem. Phys.* **101**, 4657–4667 (1994).
- ⁴⁶J. Fregoni, G. Granucci, E. Coccia, M. Persico, and S. Corni, "Manipulating azobenzene photoisomerization through strong light-molecule coupling," *Nat. Commun.* **9**, 4688 (2018).
- ⁴⁷J. Fregoni, S. Corni, M. Persico, and G. Granucci, "Photochemistry in the strong coupling regime: A trajectory surface hopping scheme," *J. Comput. Chem.* **41**, 2033–2044 (2020).
- ⁴⁸J. Fregoni, G. Granucci, M. Persico, and S. Corni, "Strong coupling with light enhances the photoisomerization quantum yield of azobenzene," *Chem.* **6**(1), 250–265 (2020).
- ⁴⁹Y. Zhang, T. Nelson, and S. Tretiak, "Non-adiabatic molecular dynamics of molecules in the presence of strong light-matter interactions," *J. Chem. Phys.* **151**, 154109 (2019).
- ⁵⁰W. Zhou, D. Hu, A. Mandal, and P. Huo, "Nuclear gradient expressions for molecular cavity quantum electrodynamics simulations using mixed quantum-classical methods," *J. Chem. Phys.* **157**(10), 104118 (2022).
- ⁵¹D. Hu, A. Mandal, B. M. Weight, and P. Huo, "Quasi-diabatic propagation scheme for simulating polariton chemistry," *J. Chem. Phys.* **157**, 194109 (2022).
- ⁵²D. Hu and P. Huo, "Ab initio molecular cavity quantum electrodynamics simulations using machine learning models," *J. Chem. Theory Comput.* **19**, 2353–2368 (2023).
- ⁵³P. V. Parandekar and J. C. Tully, "Detailed balance in Ehrenfest mixed quantum-classical dynamics," *J. Chem. Theory Comput.* **2**(2), 229–235 (2006).
- ⁵⁴J. E. Subotnik, A. Jain, B. Landry, A. Petit, W. Ouyang, and N. Belonzi, "Understanding the surface hopping view of electronic transitions and decoherence," *Annu. Rev. Phys. Chem.* **67**, 387–417 (2016).
- ⁵⁵H.-D. Meyer and W. H. Miller, "A classical analog for electronic degrees of freedom in nonadiabatic collision processes," *J. Chem. Phys.* **70**(7), 3214–3223 (1979).
- ⁵⁶W. H. Miller and S. J. Cotton, "Classical molecular dynamics simulation of electronically non-adiabatic processes," *Faraday Discuss.* **195**, 9–30 (2016).
- ⁵⁷X. Sun, H. Wang, and W. H. Miller, "Semiclassical theory of electronically nonadiabatic dynamics: Results of a linearized approximation to the initial value representation," *J. Chem. Phys.* **109**, 7064 (1998).
- ⁵⁸N. Ananth, C. Venkataraman, and W. H. Miller, "Semiclassical description of electronically nonadiabatic dynamics via the initial value representation," *J. Chem. Phys.* **127**(8), 084114 (2007).
- ⁵⁹P. Huo and D. F. Coker, "Communication: Partial linearized density matrix dynamics for dissipative, non-adiabatic quantum evolution," *J. Chem. Phys.* **135**(20), 201101 (2011).
- ⁶⁰P. Huo and D. F. Coker, "Semi-classical path integral non-adiabatic dynamics: A partial linearized classical mapping Hamiltonian approach," *Mol. Phys.* **110**(9–10), 1035–1052 (2012).
- ⁶¹S. J. Cotton and W. H. Miller, "Symmetrical windowing for quantum states in quasi-classical trajectory simulations: Application to electronically non-adiabatic processes," *J. Chem. Phys.* **139**, 234112 (2013).
- ⁶²S. J. Cotton and W. H. Miller, "Symmetrical windowing for quantum states in quasi-classical trajectory simulations," *J. Phys. Chem. A* **117**(32), 7190–7194 (2013).
- ⁶³C.-Y. Hsieh and R. Kapral, "Nonadiabatic dynamics in open quantum-classical systems: Forward-backward trajectory solution," *J. Chem. Phys.* **137**(22), 22A507 (2012).
- ⁶⁴C.-Y. Hsieh and R. Kapral, "Analysis of the forward-backward trajectory solution for the mixed quantum-classical Liouville equation," *J. Chem. Phys.* **138**(13), 134110 (2013).
- ⁶⁵G. Stock and M. Thoss, "Semiclassical description of nonadiabatic quantum dynamics," *Phys. Rev. Lett.* **78**(4), 578–581 (1997).
- ⁶⁶M. Thoss and G. Stock, "Mapping approach to the semiclassical description of nonadiabatic quantum dynamics," *Phys. Rev. A* **59**, 64–79 (1999).
- ⁶⁷J. E. Runeson and J. O. Richardson, "Spin-mapping approach for nonadiabatic molecular dynamics," *J. Chem. Phys.* **151**(4), 044119 (2019).
- ⁶⁸J. E. Runeson and J. O. Richardson, "Generalized spin mapping for quantum-classical dynamics," *J. Chem. Phys.* **152**(8), 084110 (2020).
- ⁶⁹D. Bossion, W. Ying, S. N. Chowdhury, and P. Huo, "Non-adiabatic mapping dynamics in the phase space of the SU(N) Lie group," *J. Chem. Phys.* **157**, 084105 (2022).
- ⁷⁰J. R. Mannouch and J. O. Richardson, "A partially linearized spin-mapping approach for nonadiabatic dynamics. I. Derivation of the theory," *J. Chem. Phys.* **153**(19), 194109 (2020).
- ⁷¹J. R. Mannouch and J. O. Richardson, "A partially linearized spin-mapping approach for nonadiabatic dynamics. II. Analysis and comparison with related approaches," *J. Chem. Phys.* **153**(19), 194110 (2020).
- ⁷²E. A. Coronado, J. Xing, and W. H. Miller, "Ultrafast non-adiabatic dynamics of systems with multiple surface crossings: A test of the Meyer–Miller Hamiltonian with semiclassical initial value representation methods," *Chem. Phys. Lett.* **349**(5–6), 521–529 (2001).
- ⁷³Q. Shi and E. Geva, "Nonradiative electronic relaxation rate constants from approximations based on linearizing the path-integral forward-backward action," *J. Phys. Chem. A* **108**(29), 6109–6116 (2004).
- ⁷⁴W. Zhou, A. Mandal, and P. Huo, "Quasi-diabatic scheme for nonadiabatic on-the-fly simulations," *J. Phys. Chem. Lett.* **10**(22), 7062–7070 (2019).
- ⁷⁵D. Hu, Y. Xie, J. Peng, and Z. Lan, "On-the-fly symmetrical quasi-classical dynamics with Meyer–Miller mapping Hamiltonian for the treatment of non-adiabatic dynamics at conical intersections," *J. Chem. Theory Comput.* **17**(6), 3267–3279 (2021).
- ⁷⁶B. M. Weight, A. Mandal, and P. Huo, "Ab initio symmetric quasi-classical approach to investigate molecular tully models," *J. Chem. Phys.* **155**(8), 084106 (2021).
- ⁷⁷B. Weight, A. Mandal, D. Hu, and P. Huo, "Ab initio spin-mapping non-adiabatic dynamics simulations of photochemistry," *chemRxiv:10.26434/chemrxiv-2024-4hzlj-v2* (accessed March 18, 2025).
- ⁷⁸K. Miyazaki and N. Ananth, "Nonadiabatic simulations of photoisomerization and dissociation in ethylene using ab initio classical trajectories," *J. Chem. Phys.* **159**, 124110 (2023).
- ⁷⁹Y. Liu, E. Mulvihill, and E. Geva, "Combining the generalized quantum master equation approach with quasiclassical mapping Hamiltonian methods to simulate the dynamics of electronic coherences," *J. Chem. Phys.* **161**, 164101 (2024).
- ⁸⁰Z. Liu, N. Lyu, Z. Hu, H. Zeng, V. S. Batista, and X. Sun, "Benchmarking various nonadiabatic semiclassical mapping dynamics methods with tensor-train thermo-field dynamics," *J. Chem. Phys.* **161**, 024102 (2024).
- ⁸¹N. Lyu, E. Mulvihill, M. B. Soley, E. Geva, and V. S. Batista, "Tensor-train thermo-field memory kernels for generalized quantum master equations," *J. Chem. Theory Comput.* **19**(4), 1111–1129 (2023).
- ⁸²S. N. Chowdhury, A. Mandal, and P. Huo, "Ring polymer quantization of the photon field in polariton chemistry," *J. Chem. Phys.* **154**, 044109 (2021).
- ⁸³M. A. C. Saller, A. Kelly, and E. Geva, "Benchmarking quasiclassical mapping Hamiltonian methods for simulating cavity-modified molecular dynamics," *J. Phys. Chem. Lett.* **12**(12), 3163–3170 (2021).
- ⁸⁴L. Wang, D. Trivedi, and O. V. Prezhdo, "Global flux surface hopping approach for mixed quantum-classical dynamics," *J. Chem. Theory Comput.* **10**(9), 3598–3605 (2014).
- ⁸⁵S. J. Cotton and W. H. Miller, "Trajectory-adjusted electronic zero point energy in classical Meyer–Miller vibronic dynamics: Symmetrical quasiclassical application to photodissociation," *J. Chem. Phys.* **150**, 194110 (2019).
- ⁸⁶Y. Tanimura and R. Kubo, "Time evolution of a quantum system in contact with a nearly Gaussian–Markoffian noise bath," *J. Phys. Soc. Jpn.* **58**(1), 101–114 (1989).
- ⁸⁷Y. J. Yan, "Theory of open quantum systems with bath of electrons and phonons and spins: Many-dissipaton density matrixes approach," *J. Chem. Phys.* **140**(5), 054105 (2014).

- ⁸⁸Y. J. Yan, J. Jin, R.-X. Xu, and X. Zheng, "Dissipation equation of motion approach to open quantum systems," *Front. Phys.* **11**, 110306–110327 (2016).
- ⁸⁹M. A. Zeb, P. G. Kirton, and J. Keeling, "Exact states and spectra of vibrationally dressed polaritons," *ACS Photonics* **5**(1), 249–257 (2018).
- ⁹⁰M. A. D. Taylor, A. Mandal, and P. Huo, "Light-matter interaction Hamiltonians in cavity quantum electrodynamics," *Chem. Phys. Rev.* **6**(1), 011305 (2025).
- ⁹¹M. Tavis and F. W. Cummings, "Exact solution for an N -molecule—Radiation-field Hamiltonian," *Phys. Rev.* **170**(2), 379 (1968).
- ⁹²A. O. Caldeira and A. J. Leggett, "Quantum tunnelling in a dissipative system," *Ann. Phys.* **149**(2), 374–456 (1983).
- ⁹³A. Nitzan, *Chemical Dynamics in Condensed Phases: Relaxation, Transfer and Reactions in Condensed Molecular Systems* (Oxford University Press, 2006).
- ⁹⁴E. R. Koessler, A. Mandal, and P. Huo, "Incorporating Lindblad decay dynamics into mixed quantum-classical simulations," *J. Chem. Phys.* **157**(6), 064101 (2022).
- ⁹⁵T. E. Li, A. Nitzan, and J. E. Subotnik, "Polariton relaxation under vibrational strong coupling: Comparing cavity molecular dynamics simulations against Fermi's golden rule rate," *J. Chem. Phys.* **156**(13), 134106 (2022).
- ⁹⁶J. A. Campos-Gonzalez-Angulo and J. Yuen-Zhou, "Generalization of the Tavis-Cummings model for multi-level anharmonic systems: Insights on the second excitation manifold," *J. Chem. Phys.* **156**, 194308 (2022).
- ⁹⁷U. Müller and G. Stock, "Flow of zero-point energy and exploration of phase space in classical simulations of quantum relaxation dynamics. II. Application to nonadiabatic processes," *J. Chem. Phys.* **111**(6), 77–88 (1999).
- ⁹⁸G. Tao and W. H. Miller, "Semiclassical description of electronic excitation population transfer in a model photosynthetic system," *J. Phys. Chem. Lett.* **1**, 891–894 (2010).
- ⁹⁹X. Gao, M. A. C. Saller, Y. Liu, A. Kelly, J. O. Richardson, and E. Geva, "Benchmarking quasiclassical mapping Hamiltonian methods for simulating electronically nonadiabatic molecular dynamics," *J. Chem. Theory Comput.* **16**, 2883–2895 (2020).
- ¹⁰⁰M. A. C. Saller, A. Kelly, and J. O. Richardson, "Improved population operators for multi-state nonadiabatic dynamics with the mixed quantum-classical mapping approach," *Faraday Discuss.* **221**, 150–167 (2020).
- ¹⁰¹W. C. Pfalzgraff, A. Montoya-Castillo, A. Kelly, and T. E. Markland, "Efficient construction of generalized master equation memory kernels for multi-state systems from nonadiabatic quantum-classical dynamics," *J. Chem. Phys.* **150**, 244109 (2019).
- ¹⁰²S. J. Cotton and W. H. Miller, "A new symmetrical quasi-classical model for electronically non-adiabatic processes: Application to the case of weak non-adiabatic coupling," *J. Chem. Phys.* **145**(14), 144108 (2016).
- ¹⁰³T. Ozaki, "Continued fraction representation of the Fermi-Dirac function for large-scale electronic structure calculations," *Phys. Rev. B* **75**, 035123 (2007).
- ¹⁰⁴J. Hu, R.-X. Xu, and Y. J. Yan, "Communication: Padé spectrum decomposition of Fermi function and Bose function," *J. Chem. Phys.* **133**(10), 101106 (2010).
- ¹⁰⁵J. Hu, M. Luo, F. Jiang, R.-X. Xu, and Y. J. Yan, "Padé spectrum decompositions of quantum distribution functions and optimal hierarchical equations of motion construction for quantum open systems," *J. Chem. Phys.* **134**(24), 244106 (2011).
- ¹⁰⁶Q. Shi, L. Chen, G. Nan, R.-X. Xu, and Y. J. Yan, "Efficient hierarchical Liouville space propagator to quantum dissipative dynamics," *J. Chem. Phys.* **130**(8), 084105 (2009).
- ¹⁰⁷A. Kelly, R. van Zon, J. Schofield, and R. Kapral, "Mapping quantum-classical Liouville equation: Projectors and trajectories," *J. Chem. Phys.* **136**(8), 084101 (2012).
- ¹⁰⁸M. S. Church, T. J. H. Hele, G. S. Ezra, and N. Ananth, "Nonadiabatic semi-classical dynamics in the mixed quantum-classical initial value representation," *J. Chem. Phys.* **148**, 102326 (2018).
- ¹⁰⁹S. J. Cotton and W. H. Miller, "A symmetrical quasi-classical windowing model for the molecular dynamics treatment of non-adiabatic processes involving many electronic states," *J. Chem. Phys.* **150**(10), 104101 (2019).
- ¹¹⁰W. Ying, B. X. K. Chng, M. Delor, and P. Huo, "Microscopic theory of polariton group velocity renormalization," [arXiv:2411.08288](https://arxiv.org/abs/2411.08288) (2025).
- ¹¹¹R. H. Tichauer, I. Sokolovskii, and G. Groenhof, "Tuning the coherent propagation of organic exciton-polaritons through the cavity Q-factor," *Adv. Sci.* **10**(33), 2302650 (2023).
- ¹¹²P. Fowler-Wright, B. W. Lovett, and J. Keeling, "Efficient many-body non-Markovian dynamics of organic polaritons," *Phys. Rev. Lett.* **129**(17), 173001 (2022).
- ¹¹³L. P. Lindoy, A. Mandal, and D. R. Reichman, "Investigating the collective nature of cavity-modified chemical kinetics under vibrational strong coupling," *Nanophotonics* **13**(14), 2617–2633 (2024).
- ¹¹⁴J. B. Pérez-Sánchez, A. Koner, N. P. Stern, and J. Yuen-Zhou, "Simulating molecular polaritons in the collective regime using few-molecule models," *Proc. Natl. Acad. Sci. U. S. A.* **120**(15), e2219223120 (2023).
- ¹¹⁵J. B. Pérez-Sánchez, F. Mellini, N. C. Giebink, and J. Yuen-Zhou, "Collective polaritonic effects on chemical dynamics suppressed by disorder," *Phys. Rev. Res.* **6**(1), 013222 (2024).
- ¹¹⁶A. Wu, J. Cerrillo, and J. Cao, "Extracting kinetic information from short-time trajectories: Relaxation and disorder of lossy cavity polaritons," *Nanophotonics* **13**, 2575–2590 (2024).